

Stability of Majorana zero modes with quantum optical lattices

Santiago F. Caballero-Benitez*

Departamento de Física Cuántica y Fotónica, LSCSC-LANMAC, Instituto de Física, Universidad Nacional Autónoma de México, Ciudad de México 04510, México

I analyze the emergence of Majorana zero modes (MZM) in a one dimensional ultracold fermionic system confined by an optical lattice inside a high-Q cavity. This forms a quantum optical lattice due to the cavity backaction, with emergent long range interactions controlled by the light pumped into the system and thus long range pairing. I investigate the possibility of formation and emergence of edge modes using exact diagonalization and singular value decomposition of the Hamiltonian in the Majorana representation, while computing the mass gap of the MZM. I find that under certain conditions MZM appear distinctively. This MZM have potential applications for quantum information as they are topologically protected analogous to the behaviour of the Kitaev chain.

Recent experimental developments with ultracold fermions inside high-Q cavities [1–4], motivate further analysis of the properties one might be able to control in these systems. Tailoring different regimes and phases of correlated quantum matter with bosonic realizations have been explored with interesting competition scenarios and the emergence of exotic phases of matter with the addition of optical lattices [5–9]. Ultracold Fermi systems inside cavities have been explored theoretically with [10–13] and without optical lattices [14–16]. Further, in the advent of investigating fundamental properties of fermionic systems and possible applications for quantum information of Majorana edge modes [17–19] or analog quantum simulation [20] of condensed matter light-matter hybrid systems motivates this work. As it is well known, analog superconducting systems in the tight banding limit with short range pairing present (p-wave symmetry) can support topologically protected Majorana zero modes (MZM) at the edges of the system, the Kitaev model [21]. These MZM are robust towards decoherence as they are topologically protected, and possibly robust to engineer q-bits with them.

With the above context in mind, I explore the fate of MZM in a fermionic system inside a high-Q cavity where the cavity back action induces effectively long range pairing. Thus, the light pumped into the system in combination with the cavity induced dynamics and the lattice can be used to induce emergent MZM triggered by the light-matter coupling. However, the long range character of the interaction could suppress the emergence of the modes. I explore the possibility to modify the suppression effect in the MZM in the cavity system. In the past, other finite range interacting models have been studied in connection with the emergence of MZM [25–27] portraying a complicated landscape. I find that indeed MZM can arise and with the interplay of short range interactions these can be stabilized and their amplitude maximized.

I consider the effective light-matter model of a one dimensional elongated chain of ultracold spin polarized fermions inside a single mode high-Q cavity. Following the methods in [9, 22], the low energy light-matter Hamil-

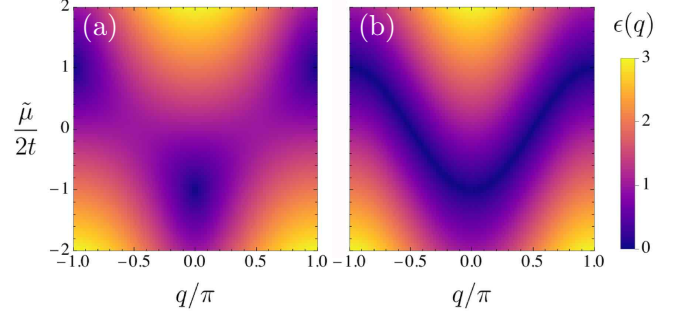


FIG. 1: Bulk dispersion relations for the Kitaev chain (a) and the system with cavity induced interactions (b) with $N_s = 10^3$.

tonian is

$$\begin{aligned} \mathcal{H} = & -\hbar\Delta_c\hat{a}^\dagger\hat{a} + t\sum_i(\hat{c}_i^\dagger\hat{c}_{i+1} + \text{H.c.}) \\ & + \frac{\hbar}{\sqrt{N_s}}\sum_i\tilde{g}_i\hat{n}_i(\hat{a}^\dagger + \hat{a}) - \mu\sum_i\hat{n}_i \end{aligned} \quad (1)$$

with the number of sites N_s . The first term is the cavity energy with the cavity-pump detuning $\Delta_c = \omega_c - \omega_p \sim \text{GHz}$. The second term is the kinetic energy with tunneling amplitude t and the last term is the light-matter interaction between the atoms (\hat{c}) and the cavity mode (\hat{a}). I assume the fermions (spinless) are trapped by an optical lattice inside a high-Q cavity. The optical lattice potential depth can be modified independently of the cavity pump modulating tunneling $t \sim \text{kHz}$ of the atoms and these are in the lowest Bloch band. I consider that the lattice is deep enough that only density coupling between light and matter is relevant [22]. The amplitudes \tilde{g}_i are the mode overlaps between the cavity mode and the spatial variation of the fermionic density in units of the Rabi frequency that emerge due to atom-photon transitions (proportional to the pump intensity). In this treatment, the transitions to excited atomic states have been adiabatically eliminated and the Wannier functions of the lowest band corresponding to the optical lattice potential have been implicitly introduced.

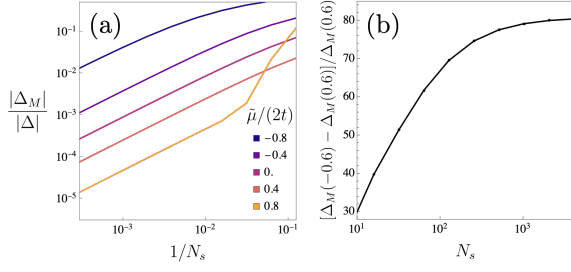


FIG. 2: (a) Mass indicator Δ_M of the MZM, with $|\tilde{\Delta}|/2t = 1$ for the imbalanced system. The MZM are localized at the edges as the number of sites N_s increases. (b) Speed factor difference between the convergence of the MZM Δ_M at $\tilde{\mu}/2t = -0.6$ and $\tilde{\mu}/2t = 0.6$.

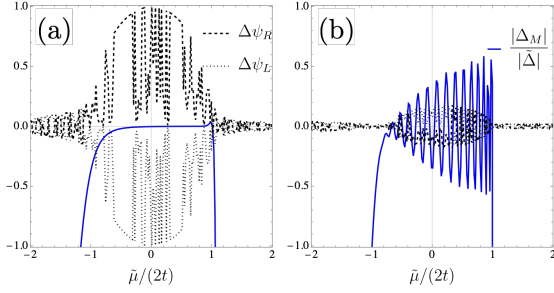


FIG. 3: Mass indicator Δ_M and differences in amplitudes of Majorana modes at the left/right edges $\Delta\psi_{L/R}$ with $N_s = 40$ and $|\tilde{\Delta}| = 2t$ for the Hamiltonians (a) $\mathcal{H}_{\text{eff}}^I$ and (b) \mathcal{H}_{eff} . For (a), MZM are present with large amplitude for $|\tilde{\mu}/2t| < 1$, $|\Delta\psi_{L/R}| \sim 1$. For (b), MZM have suppressed amplitudes. In (b) the mass indicator fails to predict the location of the MZM, as it oscillates.

I integrate out the light degrees of freedom via Hilbert space rotations [23], leading to the effective matter Hamiltonian with long range interactions induced due to cavity backaction. It follows to use the Majorana fermion mapping [21] with Majorana fermion operators given by $a_{2j-1} = e^{-i\theta/2}c_j + e^{i\theta/2}c_j^\dagger$, $a_{2j} = (e^{-i\theta/2}c_j - e^{i\theta/2}c_j^\dagger)/i$, where $\theta = \arg(\tilde{\Delta})$ is the phase of the order parameter. In Majorana language,

$$\begin{aligned} \mathcal{H}_{\text{eff}} = & -\frac{i\tilde{\mu}}{2} \sum_{j=1}^{N_s} a_{2j-1}a_{2j} \\ & + \frac{it}{2} \sum_{j=1}^{N_s-1} (a_{2j}a_{2j+1} - a_{2j-1}a_{2j+2}) \\ & + \frac{i|\tilde{\Delta}|}{2N_s} \sum_{j=1}^{N_s-2} \sum_{k=0}^{N_s-j-1} (a_{2j}a_{2(j+k)+1} + a_{2j-1}a_{2(j+k)+2}). \end{aligned} \quad (2)$$

Above it has been assumed the geometric condition of the light pumped into the system that generates constant

light-matter overlaps [28], $\tilde{g}_i = \tilde{g}$ (Diffraction maxima configuration) and later I have performed the standard mean-field decoupling of the fermionic atoms. The cavity back-action effectively induces long range paring via the long range emergent density-density interaction mediated by the photons, similar to [10]. The effective gap is $\tilde{\Delta} = \hbar\tilde{g}_{\text{eff}}\Delta$ and the effective chemical potential $\tilde{\mu} = \mu - \hbar\tilde{g}_{\text{eff}}\langle\hat{n}\rangle/2$. The gap is approximated with its mean value across the system as $\Delta \approx \sum_i \langle\hat{c}_i\hat{c}_{i+1}\rangle/N_s$ and the filling factor is $\langle\hat{n}\rangle$. The effective chemical potential and the effective gap depend on the light pumped into the system via $\tilde{g}_{\text{eff}} = \Delta_c\tilde{g}^2/(\Delta_c^2 + \kappa^2)(1 + \kappa^2/\Delta_c^2)$, with the cavity decay rate given by κ which is phenomenologically introduced and the term κ^2/Δ_c^2 is the non-adiabatic correction[23, 24]. I assume the limit where $|\Delta_c| > \kappa$ [9]. In what follows, I consider Δ as an independent parameter for simplicity [29].

The bulk dispersion of the system is given by $\epsilon(q) = \pm\sqrt{(\tilde{\mu} + 2t\cos(q))^2 + 4|\tilde{\Delta}|^2f(q)^2}$ for $-\pi \leq q \leq \pi$, with $f(q) = \sin(N_s q/2)\sin((N_s + 1)q/2)/(N_s \sin(q/2))$ [30]. The dispersion relation for the Kitaev chain and \mathcal{H}_{eff} are shown in Fig. 1. The Kitaev chain has only three Dirac points for $|\tilde{\mu}/2t| \leq 1$ at $q = 0$ ($\tilde{\mu}/2t = -1$) and $q = \pm\pi$ ($\tilde{\mu}/2t = 1$). In contrast, for \mathcal{H}_{eff} there is a continuum of Dirac points starting a $q = 0$ ($\tilde{\mu}/2t = -1$) and opening in pairs for different values of q [$q \approx \arccos(-\tilde{\mu}/2t)$] up to the $q = \pm\pi$ pair ($\tilde{\mu}/2t = 1$) for large N_s . This occurs because the cavity induced effective gap amplitude $|\tilde{\Delta}f(q)|$ has its maximum values near $q = 0$ and otherwise it almost vanishes with oscillatory behaviour. Being more precise, there are $2N_s + 1$ Dirac points in the interval $|\tilde{\mu}/2t| \leq 1$. The Dirac points are,

$$q_{\text{cav}}^D(n) = \pm \frac{(-1)^n(N_s - n + 1) + (2n - 1)N_s + n - 1}{2N_s(N_s + 1)}\pi \quad (3)$$

with $n \in \mathbb{Z}^+$ and $n \leq N_s + 1$. Starting from $q = 0$ the Dirac points open in symmetric pairs as shown in Fig. 1 (b). For finite N_s , when $\tilde{\mu} = -2t$, at the Dirac point with $q = 0$ the dispersion is massless, $\epsilon(q) \approx \pm v_F(N_s + 1)|q|$, with $v_F = |\tilde{\Delta}|$. The origin of this Dirac point is precisely the particular form of the double peak structure of $|f(q)|^2$. In the opposite limit $\tilde{\mu} = 2t$, the dispersion is also massless, with $\epsilon(q \mp \pi) \approx \pm v_F|q|$. In other finite range models [25], one recovers an equivalent dispersion for the Dirac points at $q = \pm\pi$, but the one at $q = 0$ is absent. In general near the $2N_s + 1$ Dirac points in \mathcal{H}_{eff} , I have that the dispersion is

$$\epsilon_n^D(q) \approx \pm \frac{(N_s + 1)v_F|q|}{N_s + \frac{1 - (-1)^n}{2}} \stackrel{N_s \gg 1}{\approx} \pm v_F|q| \quad (4)$$

for each $q_{\text{cav}}^D(n)$ for $2 \leq n \leq N_s + 1$ and for $q_{\text{cav}}^D(1) = 0$, $\epsilon_1^D(q) \approx \pm v_F(N_s + 1)|q|$.

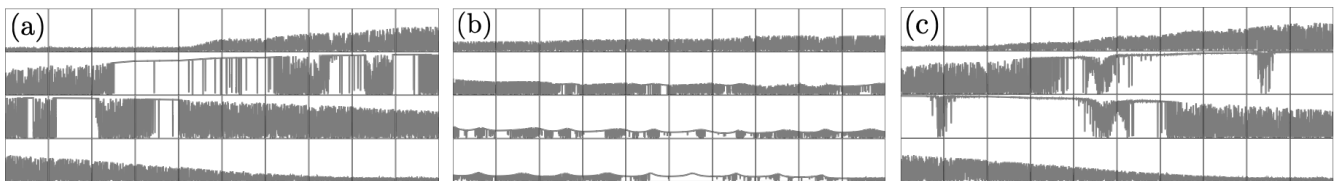


FIG. 4: The effective amplitude of edge modes $D\psi = |\Delta\psi_{L/R}| - \bar{\psi}_{L/R}|$ for (a) $\mathcal{H}_{\text{eff}}^I$, (b) \mathcal{H}_{eff} and (c) the Kitaev chain. For each Hamiltonian, each panel corresponds to an interval $[\tilde{\mu}_n^D, \tilde{\mu}_{n+1}^D]$ with the height of each panel in the interval $[0, 1]$ starting in the first panel (top left) with $\tilde{\mu}/2t = -1$ and ending in the last panel (bottom right) with $\tilde{\mu}/2t = 1$. For \mathcal{H}_{eff} and $\mathcal{H}_{\text{eff}}^I$, the asymmetric character of the MZM amplitudes across the variation of $\tilde{\mu}$ correlates with the behavior of Δ_M . It is suppressed for the negative $\tilde{\mu}$ region close to $\tilde{\mu}/2t = -1$. $\mathcal{H}_{\text{eff}}^I$ has the same Dirac points as the Kitaev chain, the windows of maximum amplitude MZM are suppressed due to the long range interactions with and without imbalance. In \mathcal{H}_{eff} the maximum amplitude is strongly suppressed. Parameters are: $N_s = 40$ and $|\tilde{\Delta}| = 2t$.

The Dirac points at $|\tilde{\mu}/2t| = 1$ in \mathcal{H}_{eff} suggest that the system with the cavity induced interaction supports zero modes with paired Majorana fermions at different sites as long as $2|t| > |\tilde{\mu}|$. In what follows, I investigate if this is the case.

The emergence of the MZM's can be studied with methods similar to [26], following the technique of [33]. I introduce the mass gap (Δ_M) parameter that quantifies effectively the amplitudes in the single particle states at different sites from the edges at the level of the commutation algebra with the Hamiltonian. First, I consider the cavity induced long-range interaction with a short range imbalance,

$$\mathcal{H}_{\text{eff}}^I = \mathcal{H}_{\text{eff}} + \frac{i|\tilde{\Delta}|}{2} r_I \sum_{j=1}^{N_s-1} (a_{2j}a_{2j+1} + a_{2j-1}a_{2j+2}), \quad (5)$$

with $r_I = 1 - 1/N_s$. The imbalance has been introduced to mimic the structure of the Kitaev chain, while considering the effect of the long range coupling between all the other sites. In principle, this imbalance could be tailored by tuning a p-wave Feshbach resonance in an actual experiment with cold atoms [31] or a similar effect could be engineered in groups of sites by means of using additional light induced modes, thus changing the geometric arrangement of the light pumped into the system, the cavity axis and the optical lattice [22, 32]. Indeed, it is found that the MZM are localized at the edges, as the mass indicator Δ_M vanishes when the number of sites increases, away from $|\tilde{\mu}/2t| = 1$, see Fig. 2. This has to do with the fact that the system only has three Dirac points, the same as the Kitaev chain. The mass indicator for the short range Kitaev chain can be computed analytically as $\Delta_M/|\tilde{\Delta}| = \tilde{\mu}/2t(-\tilde{\mu}/2t)^{N_s-1}$ when $|\tilde{\Delta}| = 2t$ [26, 33], symmetric in the speed of convergence to reach $\Delta_M=0$ around $\tilde{\mu} = 0$ as the number of sites increases. After performing numerical simulations for $\mathcal{H}_{\text{eff}}^I$ [34], the results can be fitted to,

$$\frac{\Delta_M}{|\tilde{\Delta}|} \approx -\frac{9}{10N_s} + \sum_{n=1}^9 \frac{(-1)^{n+1}\alpha_n}{N_s^{1+\delta_n}} \left(\frac{\tilde{\mu}}{2t}\right)^n, \quad (6)$$

with $\alpha_n \approx (6.16 - 11.93n + 8.9n^2 - 0.6n^3)/n^{0.82}$ and $\delta_n \approx -(17 + 2n^2) \times 10^{-3}$ for $-0.6 \lesssim \tilde{\mu}/2t \lesssim 0.6$. Thus, even though the decay is not as fast as for the Kitaev chain, the MZM will appear for $\mathcal{H}_{\text{eff}}^I$ for large number of sites as the systems moves away from $|\tilde{\mu}/2t| = 1$. Δ_M decreases faster for $0 < \tilde{\mu}/2t < 1$ compared to $-1 < \tilde{\mu}/2t < 0$. In Fig. 2, I show the maximum difference between mass indicators at $\tilde{\mu}/2t = -0.6$ (slower) and $\tilde{\mu}/2t = 0.6$ (faster) as the number of sites increases. The imbalance effect can be traced back to the fact that the combination with the long range interaction produces different signs in (6) as the system moves away from $\tilde{\mu} = 0$. This effect originates as additional sites can contribute to the low energy mode dynamics at the level of the effective equations of motion [33]. Therefore, it will be easier to observe MZM for $0 \leq \tilde{\mu} < 2t$ when short range imbalance is introduced to \mathcal{H}_{eff} .

The situation changes dramatically when \mathcal{H}_{eff} is considered without short range imbalance. I follow the same steps to compute the mass indicator as for $\mathcal{H}_{\text{eff}}^I$. I found that instead of convergence towards finding edge modes ($|\Delta_M| = 0$), $|\Delta_M|$ oscillates vigorously for $|\tilde{\mu}| < 2t$, with the frequency increasing as N_s increases. I interpret this as a signature of the fact that now the edge modes are not maximal on the whole range of $\tilde{\mu}$. So, while there exists points for $|\Delta_M| = 0$, these are not indicative of stable windows for the appearance of edge modes, see Fig. 3.

In order to confirm the above, I employ the methods shown in [35] to extract the amplitude of the edge modes via singular value decomposition (SVD) of \mathcal{H}_{eff} and $\mathcal{H}_{\text{eff}}^I$. Using SVD it is found that the amplitude of the edge modes is partially suppressed between the modes at the two extrema of the system. I interpret this imbalance as the signal for the emergence of accumulation of amplitude at the edges of the system, i.e. MZM. However, in contrast to the case of $\mathcal{H}_{\text{eff}}^I$ these are not bonafide MZM in the typical sense, i.e. the amplitudes do not maximize at the edges reaching unity, but there is a measurable imbalance with partial suppression of all other amplitudes (sites different from the edges). Looking closely at the

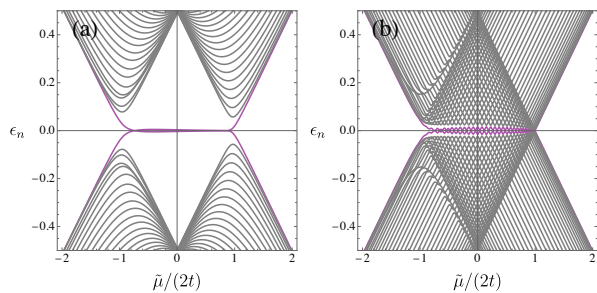


FIG. 5: Spectrum (bulk in gray) with the lowest magnitude modes (purple) in units of t for $N_s = 40$ and $|\tilde{\Delta}| = 2t$. Panel (a): $\mathcal{H}_{\text{eff}}^I$, where it can be identified there are to a very good approximation MZM in the range $|\tilde{\mu}| < 2|t|$. Panel (b): \mathcal{H}_{eff} , there are oscillations in the amplitude of the modes, thus these are not bonafide edge modes but there are values where they can have zero energy while the gap is strongly suppressed in the region $|\tilde{\mu}| < 2|t|$.

formation of the edge modes, I compute the amplitude of the edge modes for the corresponding regions in between Dirac points given by $q_{\text{cav}}^D(n)$, the chemical potential corresponding to the emergence of a possible MZM at each Dirac point is $\tilde{\mu}_n^D = -2t \cos(q_{\text{cav}}^D(n))$. Therefore, at each interval $[\tilde{\mu}_n^D, \tilde{\mu}_{n+1}^D]$ for $n \leq N_s + 1$ there is the possibility to have MZM. However, the multiplicity of the Dirac points across the whole interval $\tilde{\mu} < 2t$ complicates the analysis with respect to the Kitaev model. In the Kitaev model one can use the behavior of the Pfaffian between the Dirac points to compute the edge mode or Majorana invariant [21], for \mathcal{H}_{eff} this does not work. This is because it can predict absence or presence depending if the number of Dirac points is even or odd and it doesn't consider the damped nature of the amplitude, rendering it ambiguous. To verify the emergence of bonafide edge modes, I compute directly the distance $D\psi = |\Delta\psi_{R/L} - \bar{\psi}_{R/L}|$, which is the difference of amplitude of the edge modes and the mean value of the amplitude over all sites. In the panels of Fig. 4, I show $D\psi$ between all the intervals of the chemical potential starting for $|\tilde{\mu}| \leq 2t$. It can be seen that moving away from $|\tilde{\mu}| = 2t$, there are windows with standard edge modes (amplitude is maximal) with several regions of “oscillating suppressed amplitude edge modes” in between. Interestingly, the regular way to define the Majorana invariant does not yield conclusive evidence to identify the aforementioned windows. In the simulations it is found that sometimes counterintuitively the stability of the edge mode can extend between Dirac points (maximal between more than one panel in Fig. 4) or be partially suppressed in a region of the interval (maximal in just part of the interval in Fig. 4).

Having imbalance between the nearest neighbor part of the interaction and the interaction over all other sites stabilizes the edge modes, consistent with the mass indicator, see Fig. 3 (a). This correlates with the behavior

of the lowest magnitude modes in the spectrum Fig. 5 (a). In contrast, the energy gap to the bulk mode of the lowest magnitude modes in the case of \mathcal{H}_{eff} is suppressed Fig. 5 (b). Looking at the behaviour of the MZM in the same intervals as for \mathcal{H}_{eff} can be seen in Fig. 4. However, there are points in the $|\tilde{\mu}| \leq 2t$ interval that one can have zero energy modes Fig. 4 and Fig. 5 (b). The system with cavity induced interactions \mathcal{H}_{eff} or with imbalance $\mathcal{H}_{\text{eff}}^I$ have suppressed windows of large amplitude MZM with respect to the Kitaev chain for the same number of sites and in the same interval windows, Fig. 4. With the results from the spectrum, the mass gap and the direct computation of edge mode amplitudes it can be confirmed that indeed short range interactions can maximize the amplitude of MZM. In an experiment, the emergence of MZM could be measured directly by in-situ imaging the accumulation of density at the edges of the chain or by measuring the light in the cavity, as the number of photons is $n_{\text{ph}} = \langle \hat{a}^\dagger \hat{a} \rangle \approx |\tilde{g}_{\text{eff}}|(|\Delta|^2 + \langle \hat{n} \rangle^2/2)N_s$, when the light and matter couple, typical of the superradiant response [9].

Summarizing, I have found that MZM are present with cavity induced interactions and these can be stabilized (maximized in amplitude) with the help of short range interactions leading to similar behaviour as the MZM in the Kitaev chain. Thus, the interplay with short range interactions offers a degree of control that can help to open the energy gap to the bulk spectrum to maximize the amplitude of the MZM. In general, we expect that these MZM could be probed to be used perhaps for quantum information purposes [17–19], as using the geometric arrangement of the system (cavity and optical lattice axes) can provide sections where the pairing could be induced or suppressed as the light is pumped into the system [28], while the cavity-pump detuning provides yet another control parameter with some freedom. With the help of the light coupling one could draw the wires with pairing with the light and assemble the structures needed to have useful q-bits analogous to [17] in a single setup while modifying the structures on demand.

The phenomenology described in this letter could be explored readily in ${}^6\text{Li}$ system [1–4] or in a yet to be implemented ${}^{40}\text{K}$ system inside a high-Q cavity with the addition of an optical lattice and spin polarized fermions with current experimental setups. Ultracold atoms with an optical lattice inside a high-Q cavity have already been achieved in bosonic systems [5–9]. Perhaps, similar behaviour could be expected in analog light-induced superconducting systems [36–40] with elongated geometry arrays in some limit.

I thank J. Hofmann, H. Ritsch, P. Christodoulou and R. Gutiérrez-Jáuregui for useful discussions This work is partially supported by the grant UNAM-DGAPA-PAPIIT:IN118823.

-
- * Electronic address: scaballero@fisica.unam.mx
- [1] K. Roux et al. Strongly correlated Fermions strongly coupled to light. *Nat Commun* **11**, 2974 (2020)
 - [2] X. Zhang et al. Observation of a superradiant quantum phase transition in an intracavity degenerate fermi gas. *Science* **373**, 1359 (2021).
 - [3] K. Roux, V. Helson, H. Konishi and J. -P. Brantut. Cavity-assisted preparation and detection of a unitary fermi gas. *New J. Phys.* **23**, 043029 (2021).
 - [4] V. Helson et al. Density-wave ordering in a unitary Fermi gas with photon-mediated interactions. *Nature* **618**, 716 (2023).
 - [5] R. Landig et al. Quantum phases from competing short- and long-range interactions in an optical lattice. *Nature* **532**, 476 (2016).
 - [6] P. Zupancic, D. Dreon, X. Li, A. Baumgartner, A. Morales, W. Zheng, N. R. Cooper, T. Esslinger, and T. Donner. P-Band Induced Self-Organization and Dynamics with Repulsively Driven Ultracold Atoms in an Optical Cavity. *Phys. Rev. Lett.* **123**, 233601 (2019).
 - [7] X. Li, D. Dreon, P. Zupancic, A. Baumgartner, A. Morales, W. Zheng, N. R. Cooper, T. Donner, and T. Esslinger. First order phase transition between two centro-symmetric superradiant crystals. *Phys. Rev. Research* **3**, L012024 (2021).
 - [8] J. Klinder, H. Keßler, M. R. Bakhtiari, M. Thorwart, and A. Hemmerich. Observation of a Superradiant Mott Insulator in the Dicke-Hubbard Model. *Phys. Rev. Lett.* **115**, 230403 (2015).
 - [9] F. Mivehvar, F. Piazza, T. Donner and H. Ritsch. Cavity QED with quantum gases: New paradigms in many-body physics. *Adv. in Phys.* **70**, 1 (2021).
 - [10] A. Camacho-Guardian, R. Paredes, and S. F. Caballero-Benitez. Quantum Simulation of Competing Orders with Fermions in Quantum Optical Lattices. *Phys. Rev. A* **96**, 051602(R)(2017).
 - [11] F. Mivehvar, H. Ritsch, and F. Piazza. Superradiant topological peierls insulator inside an optical cavity. *Phys. Rev. Lett.* **118**, 073602 (2017).
 - [12] F. Schlawin, and D. Jaksch. Cavity-mediated unconventional pairing in ultracold fermionic atoms. *Phys. Rev. Lett.* **123**, 133601 (2019).
 - [13] Z. Zheng and Z.D. Wang. Cavity-induced Fulde-Ferrell-Larkin-Ovchinnikov superfluids of ultracold Fermi gases. *Phys. Rev. A* **101**, 023612 (2020).
 - [14] J. Keeling, M. J. Bhaseen, and B.D. Simons. Fermionic superradiance in a transversely pumped optical cavity. *Phys. Rev. Lett.* **112**, 143002 (2014).
 - [15] F. Piazza, and P. Strack. Umklapp superradiance with a collisionless quantum degenerate fermi gas. *Phys. Rev. Lett.* **112**, 143003 (2014).
 - [16] Y. Chen, Z. Yu, and H. Zhai. Superradiance of degenerate fermi gases in a cavity. *Phys. Rev. Lett.* **112**, 143004 (2014).
 - [17] S. Plugge, A. Rasmussen, R. Egger, and K. Flensberg. Majorana box qubits. *New J. Phys.* **19** 012001 (2017).
 - [18] P. Marra. Majorana nanowires for topological quantum computation. *J. Appl. Phys.* **132**, 231101 (2022).
 - [19] V. Kornich, X. Huang, E. Repin, and Y.V. Nazarov. Braiding and All Quantum Operations with Majorana Modes in 1D. *Phys. Rev. Lett.* **126**, 117701 (2021).
 - [20] F. Schäfer et al. Tools for quantum simulation with ultracold atoms in optical lattices. *Nat Rev Phys* **2**, 411 (2020).
 - [21] A. Yu. Kitaev. Unpaired Majorana fermions in quantum wires, *Phys.-Usp.* **44** 131 (2001).
 - [22] S. F. Caballero-Benitez, and I. B. Mekhov. Quantum optical lattices for emergent many-body phases of ultracold atoms. *Phys. Rev. Lett.* **115**, 243604 (2015). *Phys. Rev. Lett.* **115**, 243604 (2015).
 - [23] S. F. Caballero-Benitez, and I. B. Mekhov. Quantum Properties of light scattered from structured many-body phases of ultracold atoms in quantum optical lattices. *New J. Phys.* **17**,123023 (2015).
 - [24] K. Lozano-Méndez, A. H. Casares, and S. F. Caballero-Benitez. Spin Entanglement and Magnetic Competition via Long-range Interactions in Spinor Quantum Optical Lattices. *Phys. Rev. Lett.* **128**, 080601 (2022).
 - [25] D. Vodola, L. Lepori, E. Ercolessi, A.V. Gorshkov, and G. Pupillo. Kitaev Chains with Long-Range Pairing, *Phys. Rev. Lett.* **113**, 156402 (2014).
 - [26] O. Viyuela, D. Vodola, G. Pupillo, and M.A. Martin-Delgado. Topological massive Dirac edge modes and long-range superconducting Hamiltonian, *Phys. Rev. B.* **94**, 125121 (2016).
 - [27] J. Fraxanet, U. Bhattacharya, T. Grass, D. Rakshit, M. Lewenstein, and A. Dauphin. Topological properties of the long-range Kitaev chain with Aubry-André-Harper modulation. *Phys. Rev. Research* **3**, 013148 (2021).
 - [28] W. Kozłowski, S. F. Caballero-Benitez, and I.B. Mekhov. Probing Matter-Field and Atom-Number Correlations in Optical Lattices by Global Nondestructive Addressing. *Phys. Rev. A* **92**, 013613 (2015).
 - [29] In principle the gap needs to be determined self-consistently according its definition but the light parameters can be used to achieve the desired condition.
 - [30] For large number of sites the maximum contributions of $f(q)^2$ are: $\max[f(q_{\max})^2] \approx \frac{2}{3} \sin^4\left(\sqrt{\frac{3}{2}}\right) \approx 0.52$ and $q_{\max} \approx \pm \frac{2\sqrt{3}}{\sqrt{2N_s^2-1}}$.
 - [31] V. Venu et al. Unitary p-wave interactions between fermions in an optical lattice. *Nature* **613**, 262 (2023).
 - [32] S. F. Caballero-Benitez, G. Mazzucchi, and I.B. Mekhov. Quantum simulators based on the global collective light-matter interaction. *Phys. Rev. A* **93**, 063632 (2016).
 - [33] P. Fendley. Parafermionic edge zero modes in Z -invariant spin chains. *J. Stat. Mech.* P11020 (2012).
 - [34] I solve the effective linear arising from the equations of the method in [33] for different $\tilde{\mu}/2t$ and N_s .
 - [35] W. Choi, M. Knap, and F. Pollmann. Finite-temperature entanglement negativity of fermionic symmetry-protected topological phases and quantum critical points in one dimension. *Phys. Rev. B* **109**, 115132 (2024).
 - [36] D. Nicoletti, D. Fu, O. Mehio, S. Moore, A.S. Disa, G.D. Gu, and A. Cavalleri, Magnetic-Field Tuning of Light-Induced Superconductivity in Striped $\text{La}_{2-x}\text{Ba}_x\text{CuO}_4$. *Phys. Rev. Lett.* **121**, 267003 (2018).
 - [37] M. Budden et al. Evidence for metastable photo-induced superconductivity in K_3C_{60} . *Nat. Phys.* **17**, 611 (2021).
 - [38] A. Julku, J. J. Kinnunen, A. Camacho-Guardian, and G.M. Bruun. Light-induced topological superconductivity in transition metal dichalcogenide monolayers. *Phys. Rev. B* **106**, 134510 (2022).

- [39] L. Grunwald, G. Passetti, and D. M. Kennes. Dynamical onset of light-induced unconventional superconductivity—a Yukawa-Sachdev-Ye-Kitaev study. *Commun. Phys.* **7**, 79 (2024).
- [40] C. J. Eckhardt et al. Theory of resonantly enhanced photo-induced superconductivity. *Nat. Commun.* **15**, 2300 (2024).